
RESONANT THIN P-CLAD SEMICONDUCTOR LASERS

Peter S. Zory et al.

**University of Florida
Department of Electrical and Computer Engineering
319 Weil Hall
P.O. Box 116500
Gainesville, FL 32611-5500**

March 1999

Final Report

19990628 127

APPROVED FOR PUBLIC RELEASE; DISTRIBUTION IS UNLIMITED.



**AIR FORCE RESEARCH LABORATORY
Directed Energy Directorate
3550 Aberdeen Ave SE
AIR FORCE MATERIEL COMMAND
KIRTLAND AIR FORCE BASE, NM 87117-5776**

Using Government drawings, specifications, or other data included in this document for any purpose other than Government procurement does not in any way obligate the U.S. Government. The fact that the Government formulated or supplied the drawings, specifications, or other data, does not license the holder or any other person or corporation; or convey any rights or permission to manufacture, use, or sell any patented invention that may relate to them.

This report has been reviewed by the Public Affairs Office and is releasable to the National Technical Information Service (NTIS). At NTIS, it will be available to the general public, including foreign nationals.


If you change your address, wish to be removed from this mailing list, or your organization no longer employs the addressee, please notify AFRL/DELS, 3550 Aberdeen Ave SE, Kirtland AFB, NM 87117-5776.


Do not return copies of this report unless contractual obligations or notice on a specific document requires its return.

This report has been approved for publication.


DAVID J. BOSSERT
Project Manager

FOR THE COMMANDER


GREGORY J. VANSUCH, Lt. Col, USAF
Chief, Semiconductor Laser Branch


R. EARL GOOD, SES
Director, Directed Energy Directorate

REPORT DOCUMENTATION PAGE			Form Approved OMB No. 0704-0188	
Public reporting burden for this collection of information is estimated to average 1 hour per response, including the time for reviewing instructions, searching existing data sources, gathering and maintaining the data needed, and completing and reviewing the collection of information. Send comments regarding this burden estimate or any other aspect of this collection of information, including suggestions for reducing this burden, to Washington Headquarters Services, Directorate for Information Operations and Reports, 1215 Jefferson Davis Highway, Suite 1204, Arlington, VA 22202-4302, and to the Office of Management and Budget, Paperwork Reduction Project (0704-0188), Washington, DC 20503.				
1. AGENCY USE ONLY (Leave blank)	2. REPORT DATE March 1999	3. REPORT TYPE AND DATES COVERED Final Report 9/30/97 - 11/19/98		
4. TITLE AND SUBTITLE Resonant Thin P-clad Semiconductor Lasers		5. FUNDING NUMBERS C: F29601-96-C-0141 PE: 63605F PR: 3151 TA: LC WU: DL		
6. AUTHOR(S) Peter S. Zory, Carl Miester, and Jason O				
7. PERFORMING ORGANIZATION NAME(S) AND ADDRESS(ES) University of Florida Department of Electrical and Computer Engineering 319 Weil Hall P.O. Box 116500 Gainesville, FL 32611-5500		8. PERFORMING ORGANIZATION REPORT NUMBER #9 - Final Report		
9. SPONSORING/MONITORING AGENCY NAME(S) AND ADDRESS(ES) AFRL/DELS 3550 Aberdeen Ave SE Kirtland AFB, NM 87117-5776		10. SPONSORING/MONITORING AGENCY REPORT NUMBER AFRL-DE-TR-1999-1001		
11. SUPPLEMENTARY NOTES				
12a. DISTRIBUTION AVAILABILITY STATEMENT Approved for public release; distribution is unlimited.			12b. DISTRIBUTION CODE	
13. ABSTRACT (Maximum 200 words) In Phase I of the contract, the modulated cap thin p-clad (MCTC) design concept was utilized to fabricate antiguided array lasers and alpha-DFB lasers. The lateral refractive index variation required in implementing the designs was achieved by precisely modulating the thickness of the GaAs cap layer using a novel pulsed anodization/etching technique. At ten times threshold, the central lobe in the lateral far-field of the best antiguided array lasers contained about 60% of the beam power and had a divergence of about 1.6 degrees. Since the yield of such devices was only about 5%, the main effort in Phase II was to develop epitaxial design with wide "process windows" and large discrimination factors for the fundamental array mode. Alpha-DFB laser design studies showed that it was important to have a high lateral coupling/stripe width product and low loss in order to achieve high power operation. Various designs were implemented in both Phases of the contract with little success. It was concluded that the MCTC design concept was not useful for fabricating alpha-DFB lasers because the large refractive index changes required were inextricably tied to high mode losses.				
14. SUBJECT TERMS Thin p-clad lasers; antiguided array lasers; alpha-DFB lasers; modulated cap thin p-clad (MCTC) lasers; pulsed anodization/etching technique			15. NUMBER OF PAGES 40	
			16. PRICE CODE	
17. SECURITY CLASSIFICATION OF REPORT UNCLASSIFIED	18. SECURITY CLASSIFICATION OF THIS PAGE UNCLASSIFIED	19. SECURITY CLASSIFICATION OF ABSTRACT UNCLASSIFIED	20. LIMITATION OF ABSTRACT UL	

)

Table Of Contents

Report Documentation Page (SF 298)	i
List of Figures	iv
Introduction	1
Task 2 - Antiguided Array Lasers	5
Task 3 - α -DFB Lasers	18
Conclusions	30
Bibliography	31

List of Figures

Figure 1. Calculated process window for a 100 nm of element cap thickness	6
Figure 2. Calculated Process window for 18 element antiguided array	8
Figure 3. Process window of a 19 element device with 5 μm elements and 2 μm interelements for a new 3 layer cap epitaxial structure	10
Figure 4. Process window of a 19 element device with 5.5 μm elements and 1.5 μm interelements for the same epitaxial structure with above	11
Figure 5. L1936 epitaxial structure	12
Figure 6. Refractive index and mode loss of TE_0 and TE_1 vertical modes as a function of cap thickness for wafer L1936	15
Figure 7. Main lobe power percentage as a function of the ratio $r = d/s$	15
Figure 8. Mode loss and effective index vs cap thickness for the new structure	18
Figure 9. Reflection spectrum	19
Figure 10. Lateral view of a segment of an α -DFB structure	20
Figure 11. Mode gain vs mode index of the near resonant lateral modes of the α -DFB structure	22
Figure 12. New 3 layer cap wafer design	24
Figure 13. Lateral mode spectrum of a MCTC α -DFB laser structure	27
Figure 14. Current and power vs time for short as grown Fabry-Perot lasers from wafer #759	28

Introduction

On this contract, we designed and built Modulated Cap Thin P-Clad (MCTC) Antiguided Array (AGA) lasers and MCTC angled grating distributed feedback (α -DFB) lasers. These efforts were performed under tasks 2 and 3 of the contract, respectively.

In designing MCTC antiguided array lasers, there are two major constraints on epitaxial design: a wide "process window" and large array mode discrimination. In order to obtain these objectives, a three-layer cap design with a large interelement loss was grown and lasers were fabricated. However, lasing in the interelement regions verified that the desired high loss was not achieved. We believe that high mode loss was not achieved because of problems in the crystal growth. A quantitative formula for predicting etch depth resulted from additional development work on the pulsed anodization etching technique. Finally, theoretical work was done on optimizing device dimensions and cap layer thicknesses to achieve in-phase mode operation of MCTC antiguided array lasers at high power levels.

The design and fabrication of MCTC α -DFB lasers was attempted using a wafer (HDOS #734) which was designed to minimize mode loss in the MCTC structure. These lasers showed only Fabry-Perot lasing. Theoretical modeling as well as experimental results showed that it is important to have a high κW product as well as low mode loss in α -DFB lasers. In order to obtain this high κW product and a lower mode loss, a new three layer cap structure was designed which required grating etch depths of ~ 200 nm. In order to etch the required depth, the grating exposure/development was optimized using diffraction efficiency measurements. Once the grating fabrication was optimized, fabrication of α -DFB lasers was attempted with the new three layer cap wafer (HDOS #759). These lasers did not lase in an α -DFB mode. We believe that the basic reason α -DFB lasing was not achieved is due to the fact that whenever large refractive index changes are present, the accompanying losses are unacceptably high.

[Task 2] MCTC Antiguided Array (AGA) lasers

We have found that the yield of in-phase devices goes way down (a few %) when we make arrays with 20 or more elements. In order to understand this and design around it, we have created the concept of a "process window" for making MCTC antiguided array lasers. Using these ideas, a new structure has been designed that should greatly improve in-phase yield when implemented.

There are two major constraints on epitaxial design: a wide "process window" and large array mode discrimination. We demonstrate how the slope of the cap refractive index versus cap thickness plot and the magnitude of the loss in the interelement regions determines the "size" of the "process window". Array mode gain versus interelement cap thickness plots show how the "process window" is a function of the array element and interelement dimensions. Compromises between mode stability and the fractional amount of output power in the central lobe of the far field are explained.

Standard Fabry-Perot devices were fabricated and characterized from the new 3-layer cap material obtained from Lawrence Livermore National Lab. While devices made with the 3 layers intact had higher thresholds than devices made with the two top layers removed, the expected threshold difference was much smaller than predicted. We believe this resulted from smaller than desired loss in the quantum well loss layer. Lasing in the interelement regions verified that the desired high loss was not achieved. We believe that high mode loss was not achieved because of problems in the crystal growth.

Additional development work was done on the pulsed anodization etching technique used in the fabrication of antiguided arrays and alpha-DFB lasers. A quantitative formula for predicting etch depth was the result of this work. Two electrolyte mixtures were used during device fabrication to exploit their different merits.

Theoretical work was done on optimizing device dimensions to achieve in-phase mode operation of MCTC antiguided array lasers at high power levels. Device performance goals place constraints on both the element and interelement refractive index step and array dimensions. Competition between vertical modes determines the acceptable range for the index step. The

widths of the element and interelement regions place constraints on the output power contained in the main lobe.

Finally, a procedure is described for optimizing the array dimensions and cap layer thicknesses. The optimized interelement cap thickness, calculated using the resonance coupling condition, should be compared with that calculated using process window considerations.

[Task 3] MCTC Angled Grating α -DFB

The fabrication of MCTC α -DFB lasers requires the etching of deeply grooved gratings. To this end, we modified the pulsed anodization etching process. In order to reduce the loss in the laser structure, a new epitaxial wafer was ordered from HDOS. Modeling of α -DFB lasers was performed, including the relationships between coupling coefficient, mode discrimination, mode loss, and length sensitivity.

Fabry-Perot lasers with a thinned cap layer were fabricated to test the quality of the new laser wafer grown at HDOS (Wafer #734). The high threshold and low slope efficiency indicated that the thick cap produced moderate loss as expected.

Next, fabrication of α -DFB lasers was attempted, however, only lasing in Fabry-Perot modes was observed. We believe that the lack of lasing in the desired α -DFB modes was a result of low κW product, which produced low confinement for the high order modes and sensitivity to cavity length variations, and higher than desired mode loss. We have designed a new three-layer cap structure in which the κ value can be increased, while maintaining low mode loss.

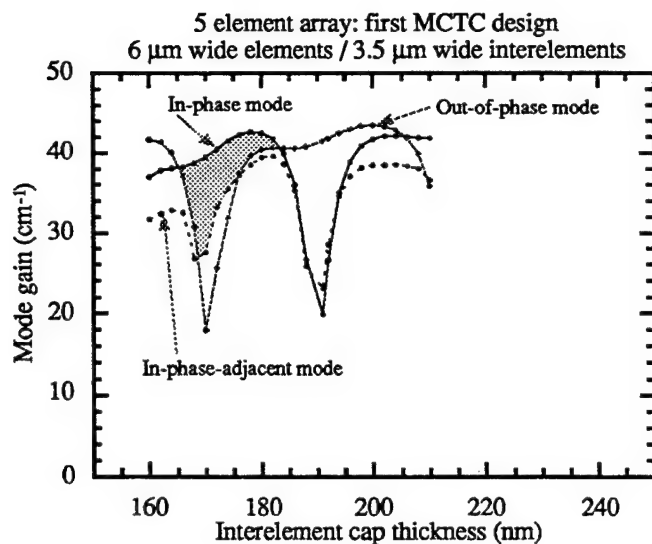
A process for production of repeatable photoresist (PR) gratings was developed. We determined that repeatable PR gratings were characterized by a range of acceptable diffraction efficiencies. Using our ability to characterize PR gratings, the grating exposure/development process was optimized by more exactly controlling the development time. An analytical formula to determine the grating etch depth using the measured diffraction efficiency was derived. Finally, theoretical work on modeling α -DFB modes, which included gratings outside the stripe region, was performed in order to optimize the new three layer cap structure.

Concluding the optimization of the grating etching procedure for the deeper etches required for the new three layer cap structure, an analytic formula for grating etch depth as a function of time was derived. Using the new wafer (HDOS #759) Fabry-Perot test lasers were fabricated using both etched and as-grown cap layers. The lasers with an etched cap performed as expected. On the other hand, the lasers processed using the as-grown wafer, were characterized by a lasing "turn-off" behavior for short cavity lengths, demonstrating that the mode loss in the structure was high. α -DFB lasers were fabricated using both new and old laser wafers, but the devices did not lase. We attribute this lack of lasing performance to high mode loss inherent in the MCTC laser structure.

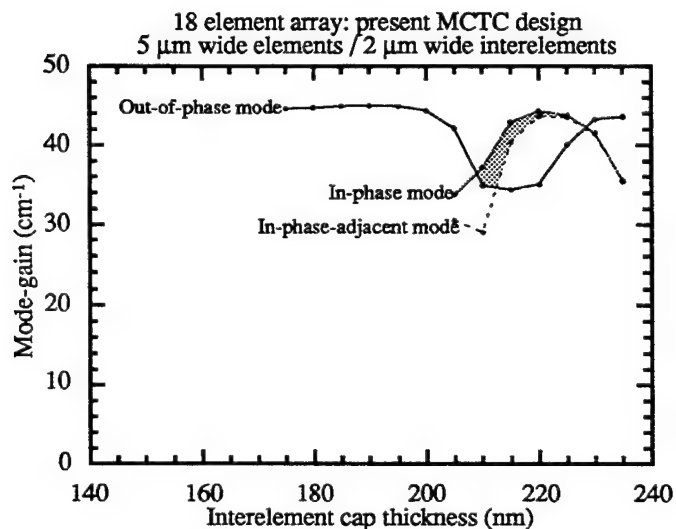
Task 2 - Antiguided Array Lasers

In order to improve our understanding of the relationship between the basic MCTC structure and the associated TE_0 refractive index variation, we have created the concept of the "process-window" for in-phase operation of MCTC antiguided array lasers. Previously, we reported that in-phase mode operation is the lowest threshold mode in a certain range of Δn_0 (effective index difference between element and interelement regions). This means that there exists a certain range of interelement cap thickness, with a fixed element cap thickness, where in-phase mode operation is the lowest threshold mode. We call this range the "process-window" for in-phase MCTC antiguided arrays. In order to have high fabrication yield and stable device operation, the process-window should be wide and the mode gain difference (mode discrimination) in the window between the in-phase and the next highest gain modes should be large.

The calculated process windows for the 5 element arrays (6 μm wide elements with 3.5 μm wide interelements) and 18 element arrays (5 μm wide elements with 2 μm wide interelements) made previously, are shown in Fig.1. Due to the limitation of our simulation program, an 18 element case was calculated instead of a 23 element case (the actual device). However, we believe that the result of the 18 element case is sufficient to determine the size of the process-window for the 23 element case. The epitaxial layer structures of the two cases are very similar except for the clad layer thickness; the clad layer thickness of the 5 element case was 250 nm and that of the 18 element case was 465 nm. For both cases, the element cap thickness was fixed at 100 nm and the mode gains for in-phase, in-phase-adjacent, and out-of-phase modes were calculated as a function of interelement cap thickness.



(a)



(b)

Fig.1 calculated process-windows for 100 nm of element cap thickness:
(a) 5 element antiguided array with 6 μm elements and 3.5 μm interelements
(b) 18 element antiguided array with 5 μm elements and 2 μm interelements

Fig.1 explains why we had better fabrication yield for 5 element devices (more than 50%) than for 23 element devices (~5%); the process-window of the 5 element case is larger than that of the 18 element case and the mode discrimination is also better for the 5 element case. The width of the process-window, where the mode discrimination is greater than 2.5 cm^{-1} , for comparison, is about 12 nm for the 5 element case and that of the 18 element case is about 5 nm.

Since the width of the process-window is narrow, the thickness uniformity of the epitaxial layers (especially the cap layer thickness) is very crucial for in-phase device fabrication. In order to check the cap thickness uniformity, we measured the cap thickness at the center and edge sections of two MOCVD wafers grown at Hughes Danbury Optical Systems. Two different methods were used with two different wafers; Dektak measurement after etching the cap layer with the SIMS (Secondary Ion Mass Spectrometry) technique, and AFM (Atomic Force Microscope) measurement after etching the cap layer with a wet chemical etching technique. The sample measured with the SIMS technique showed 50 nm of cap thickness difference between the center (200 nm) and edge (150 nm) sections and the other sample measured with the wet chemical etching showed 35 nm of variation (center: 210 nm, edge: 175 nm). Along with the narrow process-window, this cap thickness non-uniformity resulted in the low yield of the 23 element device fabrication .

To improve the fabrication yield and to achieve stable in-phase mode operation, a new epitaxial structure for MCTC antiguided array lasers has been designed. The calculated process-window for an 18 element device with this new structure is shown in Fig.2. For this case, the element cap thickness is fixed at 50 nm. The process-window width is about 24 nm which is about 5 times wider than that of the previous 18 element case, and the mode discrimination, which is an indication of stable in-phase operation, is also greatly improved.

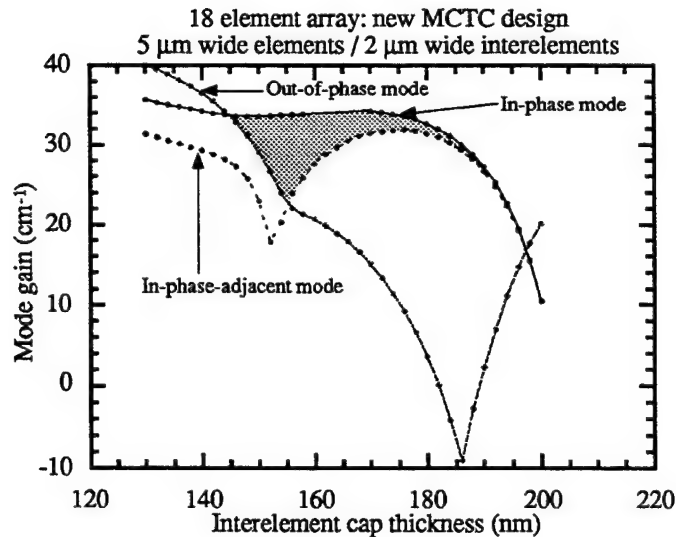


Fig. 2 calculated process-window for 18 element antiguided array (5 μm elements and 2 μm interelements) with a new epitaxial structure: element cap thickness is 50 nm.

Based on the “process-window” concept for in-phase mode operation, we have specified two major conditions for designing an epitaxial structure of MCTC antiguided array lasers. The first condition is for a wide process-window, which is related to the slope of the “refractive index vs. cap thickness” curve. This can be done by using ternary material (such as AlGaAs) as one of the layers in a multi-layer cap structure. By changing mole fractions of the ternary material, the refractive index of the layer can be changed, which leads to a change in the slope of the refractive index vs. cap thickness curve. The condition for stable in-phase operation in the process-window range is to have a high mode loss in the interelement regions, which results in large array mode discrimination. In principle, by using an active quantum well (QW) layer for a cap layer, the mode loss can be very high in the interelement regions due to band-to-band absorption loss in the

cap layer. However, there are some limitations to using active QW material for a cap layer. If the absorption loss is beyond a certain value (it depends on the index profiles of epitaxial layers and wavelength), the mode intensity in the cap layer cannot be built up enough to give sufficient index change as the cap thickness is increased. In order to avoid this problem, a thin absorption loss layer can be sandwiched between two other cap layers, but the absorption loss layer should be thicker than the QW gain layer to ensure band-to-band absorption in the loss layer. As the loss layer thickness increases, a larger mode loss is obtained, but the index slope is also increased (which leads to a narrower process-window) because the refractive index of the loss layer is higher than those of other layers. Therefore, the mole fraction of the ternary material and the loss layer thickness should be optimized together to obtain a wide process-window with large array mode discrimination.

With the idea of the above three cap-layer structure, a new epitaxial structure for MCTC anti-guided array lasers has been designed. The cap layers of the structure are 100 nm p^+ -GaAs lower cap layer, 15 nm $\text{In}_{0.15}\text{Ga}_{0.85}\text{As}$ loss layer, and 270 nm $p\text{-Al}_{0.2}\text{Ga}_{0.8}\text{As}$ upper cap layer. The p-clad thickness is 300 nm. The calculated process-window for a 19 element device (5 μm wide elements with 2 μm wide interelements) with this structure is shown in Fig.3. For this calculation, 10000 cm^{-1} absorption loss was assumed for the InGaAs loss layer, and the element cap thickness was fixed at 50 nm. The process-window width (where array mode discrimination is larger than 2 cm^{-1}) is about 28 nm, which is large enough for a high fabrication yield. The maximum array mode discrimination is about 7.5 cm^{-1} .

We have also noticed that the array mode discrimination is a strong function of the interelement dimension because of the lateral array mode confinement effect in the interelement regions. As shown in Fig.4, the maximum array mode discrimination is reduced by a factor of two when

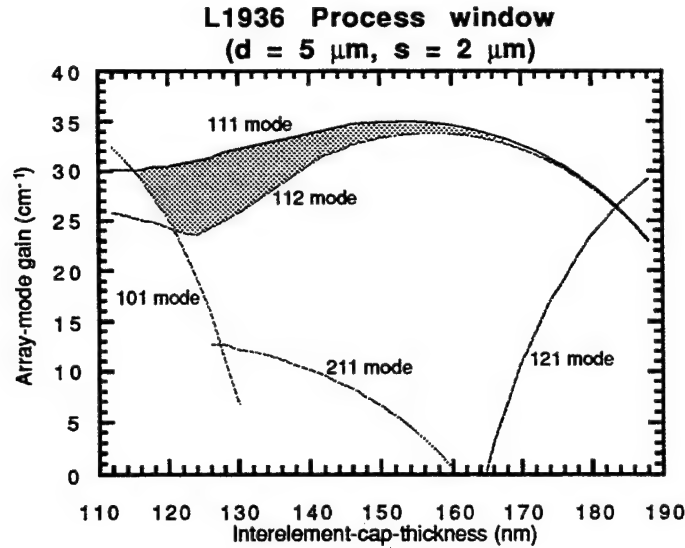


Fig.3 Process-window of a 19 element device with $5 \mu\text{m}$ elements and $2 \mu\text{m}$ interelements for a new 3 layer cap epitaxial structure

the interelement width decreases from $2 \mu\text{m}$ to $1.5 \mu\text{m}$, while maintaining the same array period ($7 \mu\text{m}$). The reason for this can be explained as follows. The lateral array mode confinement in the interelement regions decreases when the interelement width is reduced, and so does the array mode loss in the interelement regions. Since the overall array mode gain is the difference between the array mode gain in the element regions and the array mode loss in the interelement regions, and the major difference in the overall array mode gain between two array modes comes from the difference in the array mode loss in the interelement regions, the array mode discrimination decreases when the interelement width is reduced. On the contrary, the process-window width doesn't change much and the window position is shifted to larger interelement thicknesses. This is due to the fact that the window width mainly depends on the index slope and the window position is determined by the resonance coupling condition which is related to the element and interelement dimensions.

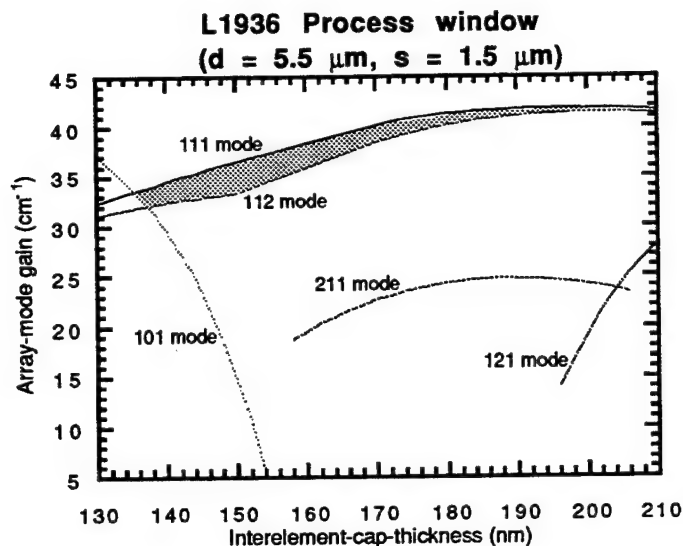


Fig.4 Process-window of a 19 element device with $5.5 \mu\text{m}$ elements and $1.5 \mu\text{m}$ interelements for the same epitaxial structure with the above

Considering the above results, to achieve stable in-phase mode operation, the interelements should be relatively wide and have large interelement loss. However, when the interelement dimension increases, the output power percentage in the main lobe of far field pattern decreases. Unless interelement loss is high enough to get sufficient mode discrimination, we have to compromise between wider width for stable operation and narrower width for higher power in the main lobe.

A wafer (L1936) for MCTC antiguided array lasers was grown at the Lawrence Livermore National Lab. The epitaxial structure of the wafer included the newly designed three cap layer structure mentioned previously. The detailed structure of the wafer is shown in Fig.5. Before MCTC antiguided array lasers were made from the wafer, the wafer was tested to check if it had the high interelement loss for which it was designed. Standard $50 \mu\text{m}$ stripe lasers with two different cap thicknesses (50 nm and 385 nm) were made. For the 50 nm cap lasers, all the upper cap layer (270 nm $\text{Al}_{0.2}\text{Ga}_{0.8}\text{As}$) and the loss layer (15 nm $\text{In}_{0.15}\text{Ga}_{0.85}\text{As}$) were etched off, and

p-cap: $\text{Al}_{0.2}\text{Ga}_{0.8}\text{As}$	270 nm
SQW: $\text{p-In}_{0.15}\text{Ga}_{0.85}\text{As}$	15 nm
p^+ -cap: GaAs	100 nm
p-clad: $\text{Al}_{0.6}\text{Ga}_{0.4}\text{As}$	300 nm
p-guide: $\text{Al}_{0.3}\text{Ga}_{0.7}\text{As}$	200 nm
barrier: GaAs	7 nm
SQW: $\text{In}_{0.15}\text{Ga}_{0.85}\text{As}$	8 nm
barrier: GaAs	7 nm
n-guide: $\text{Al}_{0.3}\text{Ga}_{0.7}\text{As}$	200 nm
n-clad: $\text{Al}_{0.6}\text{Ga}_{0.4}\text{As}$	1400 nm

Fig. 5. L1936 epitaxial structure

an additional 50 nm of the lower cap layer (GaAs) was removed. For the 385 nm cap lasers, no layers were removed. The 50 nm cap lasers had about 100 mA threshold current (600 μm cavity length). Based on this result and theoretical calculations, assuming the loss layer functioned as designed, the 385 nm cap lasers (600 μm cavity length) were expected to have a threshold current of ~ 1200 mA. However, they had a threshold current of 250 mA, which corresponded to a calculation in which there was no loss in the loss layer. This preliminary result demonstrated that there was no loss layer effect with the wafer, which made us doubt whether the cap InGaAs QW layer (loss layer) was well defined or whether the loss in the loss layer was non-saturable.

Although the initial test results were not promising, MCTC antiguided array lasers were made from the wafer and as expected, the results were negative. The cap thickness of 5 μm wide elements was 50 nm and the 2 μm wide interelement cap thickness was processed for 245 nm and 265 nm. All the devices showed lasing action in the interelement regions, as well as in the element regions, which indicated that the loss in the interelement regions was too small. With this result, we are inclined to believe that the cap InGaAs QW layer (loss layer) and the upper cap AlGaAs layer might not be properly grown. We have ruled out the possibility that the loss is saturable based on the MCTC antiguided array device geometry.

During the fabrication of the MCTC antiguided array lasers, further study of pulsed anodization etching was done. It was found that the etch rate for pulsed anodization was not constant with time. Etch depth, $h(t)$, could be predicted with the following expression:

$$h(t) = v_0 t + h_0 (1 - e^{-\alpha t}).$$

The parameters, v_0 , h_0 , and α , depend on anodization materials (GaAs or AlGaAs) and electrolytes (GWA or GWA841; GWA is composed of 40 part ethylene glycol, 20 part DI water and 1 part 85% phosphoric acid, and the ratio of those ingredients for GWA 841 is 8:4:1). Once those parameters were determined based on experiments for a given anodization material with an electrolyte, the formula produced accurate predictions (within 10 nm) for etch depth of the material. The lapse of time after making the electrolyte was also an important parameter for pulsed anodization etching; etch rate of a fresh electrolyte was higher than that of an aged electrolyte. We believe that the time required for chemical stabilization of the ingredients is 24 hours. The anodization results were quite consistent and reproducible using electrolytes between two and four days old. Hence, for device fabrication, the electrolytes were made a day before they were used.

The electrolyte GWA is a slower and more precise etchant than GWA841, so both electrolytes are used to fabricate MCTC antiguided array lasers due to their merits. GWA is used to perform a slower etch of the whole wafer surface to obtain the right cap thickness for interelement regions, which must be precise. For the groove etching of element regions, we use GWA841 because it is faster and produces smaller undercut, resulting in better control of array dimensions and steeper side walls.

The basic constraints in designing MCTC antiguided array lasers relate to element and interelement cap thicknesses and their widths. The first constraint is on the refractive index difference (Δn_0) for the TE_0 vertical mode between the element and interelement regions. The index step, Δn_0 , should be large enough ($\Delta n_0 \geq 0.01$) for the devices to be insensitive to thermal and/or carrier induced refractive index variations; this constraint places a lower limit on Δn_0 and hence the interelement cap thickness. The second constraint, which places an upper limit on Δn_0 , is that the interelement regions should not lase. As the cap thickness of a thin p-clad structure is increased, both the effective index and the loss of the TE_0 mode are also increased. Eventually, the loss of the TE_0 mode becomes larger than that of the TE_1 vertical mode and the TE_1 mode lases (see Fig. 6). Hence, the cap thickness of the interelement regions should be thin enough that the TE_1 mode cannot lase; this places an upper limit on the interelement cap thickness and hence Δn_0 . The third constraint regards element and interelement widths. Element width (d) should accommodate only a single fundamental lateral mode for in-phase array mode operation, which limits d to a maximum value (d_{\max}). Interelement width (s) is limited to a minimum value (s_{\min}) by photolithography and consideration of array mode discrimination. The ratio r ($r=d/s$) directly affects the fraction of the output power in the main lobe of the far field pattern, with a larger ratio producing higher power in the main lobe (see Fig. 7). On the contrary, array mode discrimination decreases as r increases, as we have explained previously.

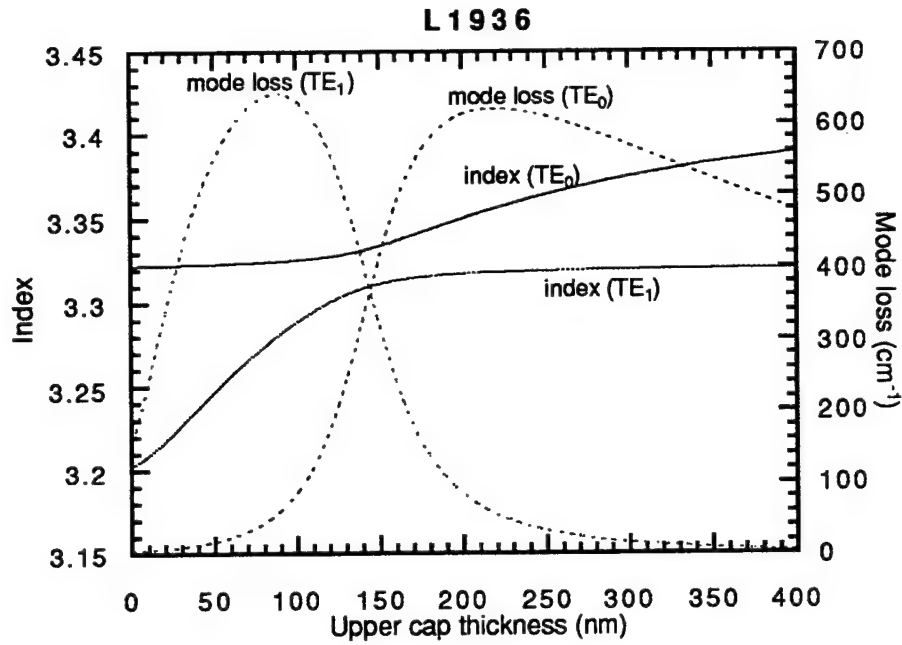


Fig. 6. Refractive index and mode loss of TE₀ and TE₁ vertical modes as a function of cap thickness for wafer L1936.

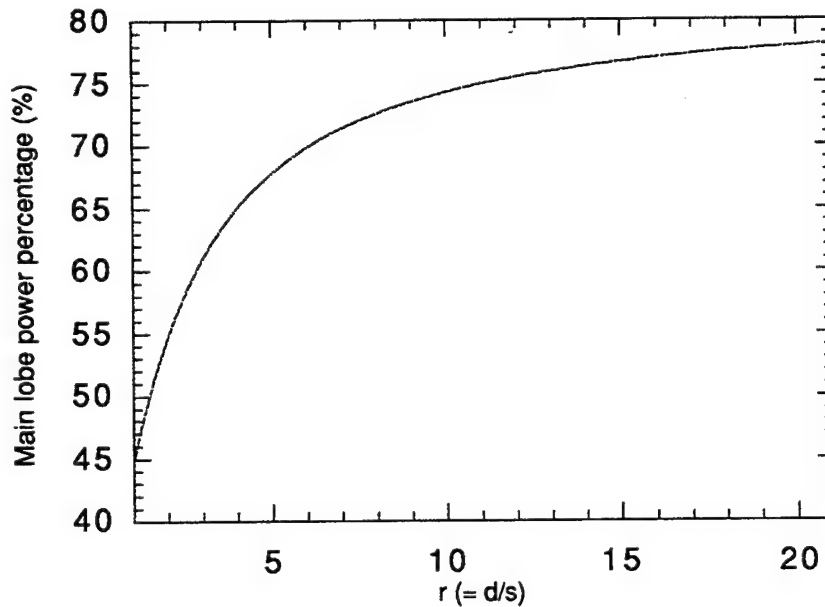


Fig. 7. Main lobe power percentage as a function of the ratio $r=d/s$, assuming that the lateral field distribution of an element is sinusoidal.

Once Δn_0 , d_{\max} and s_{\min} are determined from the basic constraints, optimum values for d and s can be calculated using the following procedure. The resonance coupling condition is:

$$\left(\frac{m\lambda_0}{2s}\right)^2 - \left(\frac{q\lambda_0}{2d}\right)^2 = n_i^2 - n_e^2 \equiv \Delta n_0^2, \quad (1)$$

where λ_0 is the laser emission wavelength, m and q are the numbers of lateral standing wave peaks in the interelement and element regions respectively (q should be 1 and m should be an odd number for in-phase coupling) and n_i and n_e are the refractive indices in the interelement and element regions respectively. An optimum range of r can be calculated by using equation (1) and the third constraint ($d \leq d_{\max}$, $s_{\min} \leq s$, and $r=d/s$) along with Δn_0 . Combining these equations, one obtains:

$$\frac{1}{\sqrt{m^2 - (2s_{\min}/\lambda_0)^2 \Delta n_0^2}} \leq r \leq \frac{\sqrt{1 + (2d_{\max}/\lambda_0)^2 \Delta n_0^2}}{m}. \quad (2)$$

From the above range of r , a desired minimum value r_{\min} can be chosen, and an optimum range of s calculated using the resonance condition again;

$$\left(\frac{\lambda_0}{2}\right) \sqrt{\frac{1}{\Delta n_0^2} \left(m^2 - \frac{1}{r_{\min}^2}\right)} \leq s \leq md_{\max} / \sqrt{1 + \left(\frac{2d_{\max}}{\lambda_0}\right)^2 \Delta n_0^2}. \quad (3)$$

Then, a desired value of s is chosen from the above range and a corresponding value of d is calculated as follows;

$$d = s / \sqrt{m^2 - \left(\frac{2s}{\lambda_0}\right)^2 \Delta n_0^2}. \quad (4)$$

After d and s are thus chosen, the corresponding process window should be calculated to determine the correspondence, or lack thereof, between the resonance condition and the maximum array mode discrimination, thus optimizing the interelement cap thickness.

From the inequality (2), it should be noticed that an array mode with a larger m number produces a smaller r value, and therefore, lower power in the main lobe of the far field pattern. Therefore, a smaller m number array mode is desirable.

Task 3 - α -DFB Lasers

Fabrication of α -DFB lasers with a grating period of $0.55\ \mu\text{m}$ and an angle of $\sim 75^\circ$ was attempted using wafers (#697 and #698) grown at HDOS. These lasers lased in a Fabry-Perot mode and no α -DFB lasing was observed. We believed that the problem with these devices was the loss modulation in the structure. In order to minimize the loss modulation in the structure, a new wafer was designed which allows for a change in refractive index with a minimization of the change in mode loss. For the previous designs, the difference in mode loss between the low and high index regions was $\sim 20\ \text{cm}^{-1}$. Figure 8 shows the mode loss and index plots for this new

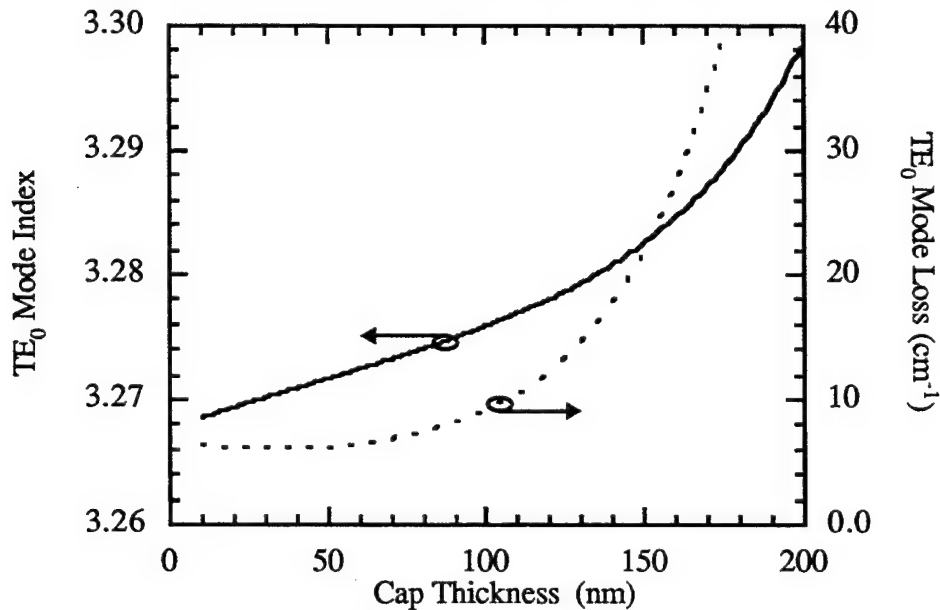


Figure 8. Mode loss and effective index vs. cap thickness for the new structure

structure. As the figure shows, a reasonable index modulation (~ 0.005) can be achieved with a 50 nm etch, and only a $5\ \text{cm}^{-1}$ loss modulation results.

We also attempted to model the lateral mode of the α -DFB structure using simple multi-layer stack theory. Since the modes of the α -DFB are "leaky," it should be possible to excite them

with a plane wave which is incident on the grating structure at the appropriate angle. Figure 9(a)

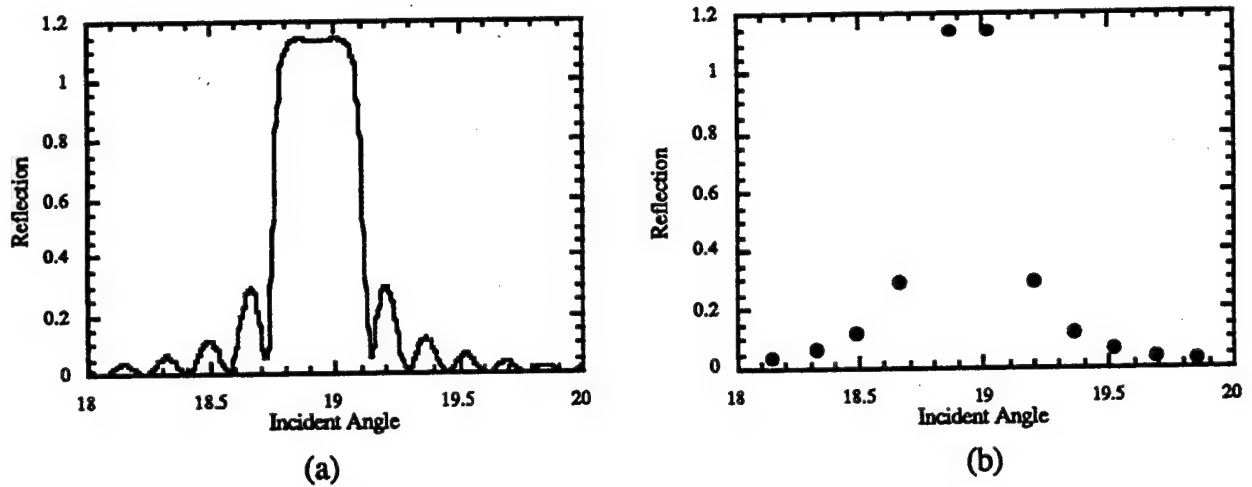


Figure 9. (a) Reflection spectrum of a grating structure which is 150 μm wide with a gain of 25 cm^{-1} in the grating region
(b) Reflection peaks vs. incident angle for the spectrum shown in Fig 2(a)

shows the reflection vs. incident angle for a grating region 150 μm wide with a gain of 25 cm^{-1} and Fig 9(b) shows the peak reflection points vs. incident angle. The problem with this approach is computing the mode gain from the reflection spectrum. An alternative approach to modeling the lateral modes using the transfer matrix method was adopted.

Here, we briefly discuss a theoretical analysis of lateral modes of waveguides having angled grating. The lateral view of a typical waveguide used in α -DFB lasers is shown in Fig.10. Starting from the wave equation, it can be shown that the field and its derivation within each layer of the waveguide are given by:

$$\begin{pmatrix} E_n \\ E'_n \end{pmatrix} = M_n (y - y_n) \begin{pmatrix} a_{bn} \\ a_{fn} \end{pmatrix}$$

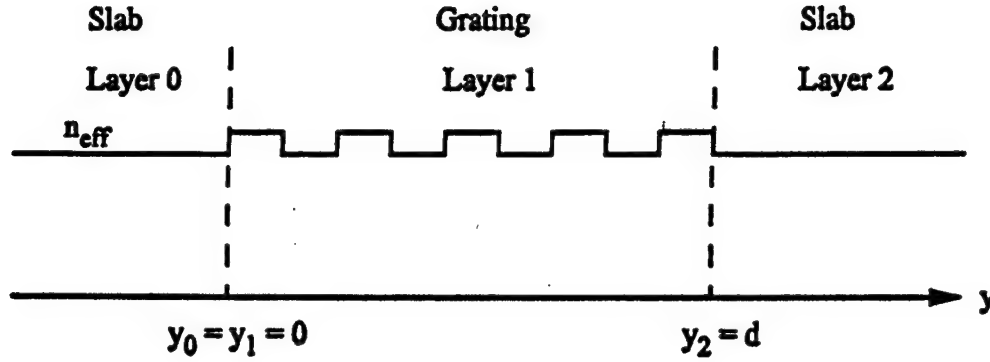


Figure 10. Lateral view of a segment of an α -DFB structure.

where $a_{bn}(a_{fn})$ is the coefficient of the backward (forward) traveling wave, y_n is the beginning of n^{th} layer,

$$M_{n11}(y) = \exp(ik_n y)$$

$$M_{n12}(y) = \exp(-ik_n y)$$

$$M_{n21}(y) = ik_n \exp(ik_n y)$$

$$M_{n22}(y) = -ik_n \exp(-ik_n y)$$

for a slab layer,

$$M_{n11}(y) = [\exp(i\sigma_n y) + r_n \exp(-i\sigma_n y)] \exp(iS_n y)$$

$$M_{n12}(y) = [-r_n \exp(i\sigma_n y) + \exp(-i\sigma_n y)] \exp(-iS_n y)$$

$$M_{n21}(y) = i [(\sigma_n + S_n) \exp(i\sigma_n y) + r_n (-\sigma_n + S_n) \exp(-i\sigma_n y)] \exp(iS_n y)$$

$$M_{n22}(y) = -i [(\sigma_n - S_n) \exp(i\sigma_n y) + r_n (\sigma_n + S_n) \exp(-i\sigma_n y)] \exp(-iS_n y)$$

for a grating layer,

$k_n = [(K_{\text{mat}})^2 - \beta^2]^{1/2}$, $K_{\text{mat}} = 2\pi n_n / \lambda + i \gamma_n / 2$, $\sigma_n = 2\pi n_n \sin \theta / \lambda$, $r_n = -i\kappa / (S_n + k_n - \sigma_n)$, $S_n = [(k_n - \sigma_n)^2 - \kappa^2]^{1/2}$, λ is the wavelength in vacuum, θ is the grating resonant angle, γ_n is the n^{th} layer loss (or gain), n_n is the n^{th} layer effective index, κ is the coupling coefficient of the angled-grating, and β is the propagation constant of the mode in the longitudinal direction.

Now, by requiring the field of each lateral mode to be purely forward traveling wave at the right boundary interface (i.e., $n = 2$) and purely backward traveling wave at the left boundary interface (i.e., $n = 0$), the following dispersion equation is obtained:

$$F(\beta) = \begin{pmatrix} 1 & 0 \end{pmatrix} M_2^{-1}(0) M_1(d) M_1^{-1}(0) M_0(0) \begin{pmatrix} 1 \\ 0 \end{pmatrix}$$

Then, from the complex solution of the above equation, the modal gain and index of the lateral modes of the α -DFB are obtained as:

$$\gamma_m = 2 \text{Im}(\beta_m) \quad \text{and} \quad n_m = \text{Re}(\beta_m) \lambda / 2\pi$$

where the subscript m is the m^{th} lateral mode of the structure. As an example, let us consider an α -DFB structure with the following waveguide parameters: resonant wavelength, $\lambda = 980$ nm ; grating resonant angle, $\theta = 15^\circ$; coupling coefficient, $\kappa = 50 \text{ cm}^{-1}$; average effective index (assumed to be constant across the width of the waveguide), $n_n = 3.34$; grating width, $w = 300 \text{ } \mu\text{m}$; and gain of the pumped region, $\gamma_{\text{pump}} = 50 \text{ cm}^{-1}$. Figure 11 shows modal gain versus modal index of the near resonant lateral modes of the α -DFB structure. As seen from the figure, the structure has two degenerate modes at either side of the resonance. The modal

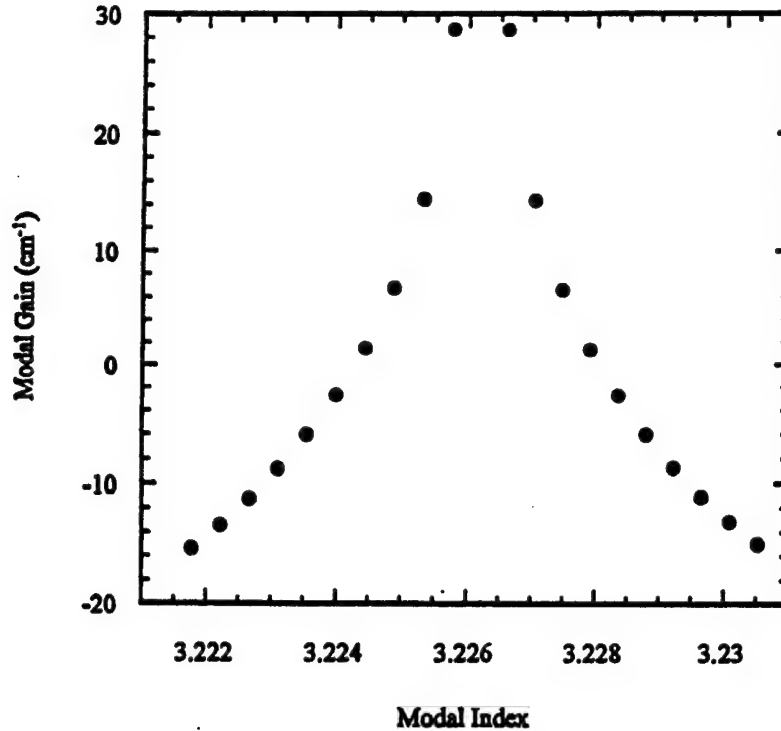


Figure 11. Mode gain vs mode index of the near resonant lateral modes of the α -DFB structure.

gain of these two modes is about 28.7 cm^{-1} while that for the next pair of degenerate modes is about 14.3 cm^{-1} . Thus, there is nearly 14.4 cm^{-1} of gain discrimination between the first two pairs of degenerate modes with the highest modal gain. Since both degenerate modes simultaneously participate in the lasing action of the α -DFB lasers, 14.4 cm^{-1} of gain discrimination indicates that α -DFB structures provide strong mode selectivity in the lateral directional.

We received a wafer (wafer #734) from HDOS grown according to the new design. Initially, FP lasers were fabricated to evaluate the material. The initial cap thickness of this wafer was $\sim 250 \text{ nm}$, and for the test devices, 100 nm of the cap was removed. $100 \mu\text{m}$ stripes were

defined with PR and electroplated. Finally, bars were cleaved with a nominal cavity length of 500 μm . For these devices with a relatively "thick" (~ 150 nm) cap the threshold current density was ~ 300 A/cm² and they had a slope efficiency of 0.14 W/A. This relatively high threshold and low slope are due to the moderate loss in this thick cap material.

Next, we attempted to fabricate α -DFB lasers. The α -DFB laser parameters were as follows: $\theta = 17^\circ$, $\Lambda = 0.49$ μm , stripe width of 150 μm , and the grating etch depth was ~ 50 nm. The devices fabricated with oxide and Ni/Au metallization outside the stripe region showed no lasing in either an α -DFB mode or any other mode of operation. Devices were also fabricated without metallization outside the stripe region, but these devices only lased in a Fabry-Perot mode between the facets.

After evaluating these fabricated devices and analyzing the theoretical mode spectrum of α -DFB devices we have come up with the following reasons for the failure of these devices.

1. In order to have the high order resonant lasing modes confined to the stripe region, the κW product must be relatively large ($\kappa W \sim 3$). In the case of these devices, the κW product was small ($\kappa W \sim 1.5$), and the high order resonant modes had significantly less mode gain than the naturally well confined low order modes. As a result, the low order modes simply oscillated internally and consumed the gain; never allowing the desirable modes to lase.
2. A low κW corresponds to a device which is relatively sensitive to cavity length variations. Theoretically, in order for the α -DFB laser to lase, the cavity length must be an integral number of exchange lengths. The exchange length in this device is inversely related to the lateral mode spacing of the resonant modes, which is related to the κW product. As κW increases, the mode spacing also increases and the exchange length

decreases. A device with a large exchange length (few exchanges in a typical 1mm device) corresponds to a device which is sensitive to cavity length variations.

3. Although this wafer (HDOS #734) was designed to minimize the imaginary component of the coupling coefficient κ , the design still had too much mode loss.

In order to obtain large κ values without introducing excessive loss (the problem with the current wafer design) we designed a new wafer with a three layer cap section. In this design, the mode interaction with the metal was controlled by a region of low refractive index material between two layers of GaAs. Figure 12 shows this new structure. Using this design, a κ of

25 nm	cap	GaAs
200 nm	cap	$\text{Al}_{0.27}\text{Ga}_{0.73}\text{As}$
50 nm	cap	GaAs
275 nm	p-clad	$\text{Al}_{0.45}\text{Ga}_{0.55}\text{As}$
150 nm	p-guide	$\text{Al}_{0.3}\text{Ga}_{0.7}\text{As}$
150 nm	n-guide	$\text{In}_{0.15}\text{Ga}_{0.85}\text{As (QW)}$ $\text{Al}_{0.3}\text{Ga}_{0.7}\text{As}$
1400 nm	n-clad	$\text{Al}_{0.6}\text{Ga}_{0.4}\text{As}$
	substrate	GaAs

Figure 12. New 3 layer cap wafer design

$\sim 300\text{cm}^{-1}$ is possible with an average mode loss of $\sim 11\text{cm}^{-1}$.

Since the new design requires etch depths of ~ 200 nm, some time was spent trying to etch

repeatable, deep gratings. In previous experiments, gratings would sometimes have a non-uniform etch pattern (especially for long etch times), such that gratings exposed in the same manner did not always etch the same. The cause of this non-repeatability could either be in the grating exposure/development (photo-resist PR gratings) or in the etching itself. Since we had the same problem with both chemical and pulsed-anodization (PA) etching, we believed that the problem was the grating exposure/development.

In order to eliminate this problem, we created a procedure to evaluate the quality of the PR gratings. The evaluation of the PR gratings involved measuring the diffraction efficiency (η) of the $q = -1$ diffracted order for a fixed angle of incidence and grating period. Samples that were measured, were then etched and a correspondence between a good, uniform etch and the η value was determined. For uniform gratings with etch depths greater than 100 nm it was determined that η should be in the range of 1.5% -2%. The reason for this range is that when the η is less than 1.5% the PR is too thin and does not work very well as a mask in the PA process, allowing some PR to be removed and the etching to be non-uniform. When $\eta > 2\%$, the PR has not been completely removed to the surface between the PR grating teeth and once again non-uniform etching results.

With the ability to evaluate PR gratings, we turned our attention to improving the exposure/development procedure. While watching several samples develop after exposure (for the same exposure time) we noticed that the developing time seemed to depend on the agitation of the solution. In order to eliminate the effect of agitation due to holding the sample by hand, we decided to stir the developer at a constant rate. Since the stirring effect is much stronger than small hand movements, the development time should no longer be determined by hand agitation. Also, it was noticed that (for the fixed exposure time and laser power) the grating pattern appears

after ~3 sec and by ~6 sec the pattern is uniform and constant until ~20 sec. After 20 sec the pattern would start to fade and eventually disappear completely. This evolution is due the developer removing the undesirable PR initially and forming a uniform grating, and then slowly starting to remove the desired sections of the PR mask. Since we want a mask in which the PR is removed to the surface between the grating teeth, but also strong enough to withstand the etching process, careful selection of development time is required. After studying the development times and the corresponding η , we determined that the development time (while the solution is being stirred) should be ~15 sec. for a constant exposure time, laser power, etc. It is important to note that since η is a function of both grating period and angle of incidence, the above procedure would be different for different grating periods.

In order to eliminate the need to profile each sample with AFM to determine the etch depth (a), we attempted to compute a from the etched η . A formula was derived for a as a function of η assuming a sinusoidal corrugation, $a = C(\Lambda, \theta) * \eta^{0.5}$, where C is a constant dependent on Λ , the grating period, and θ , the angle of incidence. Next several samples were etched and profiled with AFM, and the corresponding a was computed according to the above formula. The computed a was ~15 nm deeper than the measured value for several different etch depths. This correspondence allows us to determine a based on simple diffraction efficiency measurements. After etching several samples for different times and measuring the etch depth, the following relationship was determined: $a(t) = 14.2 + 1.5t - 0.002t^2$ where $a(t)$ is the grating etch depth and t is the etch time in seconds for etch times less than four minutes.

Work on the modeling of the lateral mode spectrum has been expanded to include gratings in both the stripe and unpumped regions. This model was used to optimize the new three layer

cap design, and figure 13 shows the theoretical lateral mode spectrum of MCTC α -DFB devices

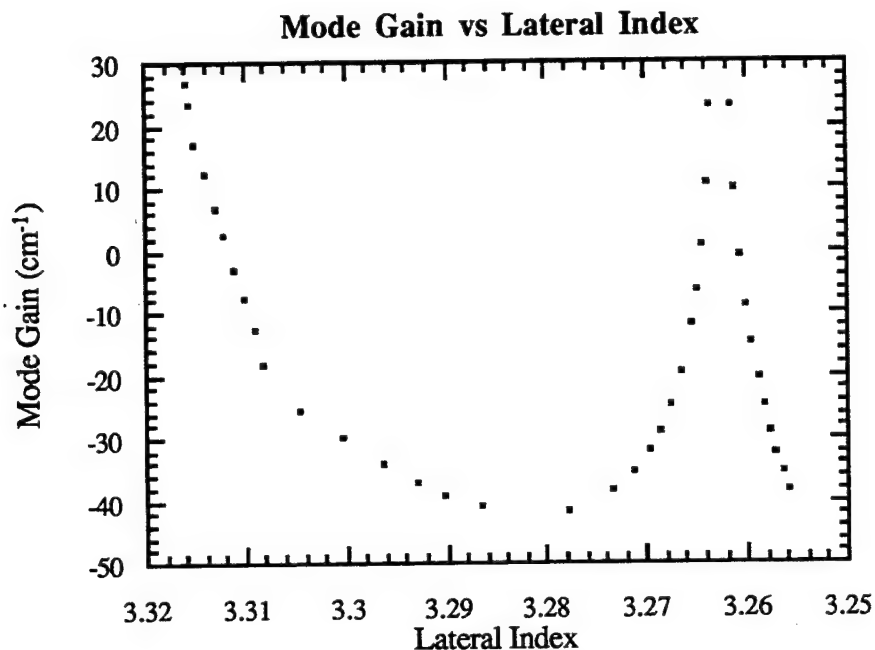


Figure 13. Lateral mode spectrum of a MCTC a-DFB laser structure with the following parameters: $\theta = 10.3$, $\kappa_{\text{stripe}} = 320 \text{ cm}^{-1}$, $\kappa_{\text{outside stripe}} = 320 \text{ cm}^{-1}$.

which based on the optimized three layer cap design. Parameters for the plot are as follows: $\theta = 10.3$, $\kappa_{\text{stripe}} = 320 \text{ cm}^{-1}$, $\kappa_{\text{outside stripe}} = 320 \text{ cm}^{-1}$.

We received a wafer grown at HDOS according to the new (3 layer) cap design (wafer #759), and initially, this wafer was processed and tested in a FP configuration to evaluate the material. Two pieces were processed; one was processed as-grown and one was etched, removing 230 nm of the cap, and then processed. The section which was etched before being processed was well behaved, and for a 575 μm length device had $J_{\text{th}} \sim 150 \text{ A/cm}^2$ and a slope of 0.26 W/A. This behavior was expected since the etched (thin cap) sample had a relatively low loss. The section which was processed as-grown was not as well behaved. For short ($L < 600 \mu\text{m}$) cavity lengths, the devices lased as shown in Figure 14. This figure shows that when current is initially applied to

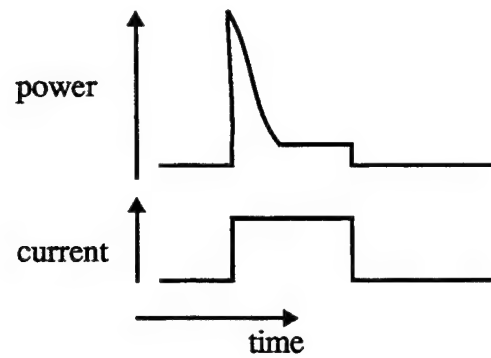


Figure 14. Current and Power vs. time for short as-grown Fabry-Perot lasers from wafer #759.

the device, it lases with a large threshold current (~ 800 mA for a $400 \mu\text{m}$ length laser) and then quickly shuts off. Devices with $L > 800 \mu\text{m}$ lased with typical power-current relationships.

We believe the reason for this lasing “turn-off” behavior is due to the loss in the as-grown wafer. Since the mirror loss is proportional to the inverse of the cavity length, a short laser has to overcome a large mirror loss in addition to the mode loss due to the structure. In this structure (as-grown), the mode loss is high ($\sim 20 \text{ cm}^{-1}$ calculated) and therefore the threshold gain and current are also high. The “turn-off” behavior is due to the fact that the mode loss for the fundamental mode in this structure increases as the cap heats up due to the contact resistance. Initially, the laser can lase, but with a high threshold current, and then as the cap temperature increases, the mode loss increases, and the laser shuts-off.

Internal mode loss (α_i) and injection efficiency (η_i) were computed from measurements of the as-grown material for cavity lengths $> 800 \mu\text{m}$ and found to be $\alpha_i = 32 \text{ cm}^{-1}$ and $\eta_i = 0.82$.

Next we attempted to fabricate α -DFB lasers. Lasers were attempted using wafer #759 as well as wafer #734. Although wafer #734 had not been successful in the past, we had never etched this wafer with gratings deeper than 50 nm . The α -DFB laser parameters were as follows: $\theta \sim 10.5^\circ$, $\Lambda \sim 0.78 \mu\text{m}$, and a stripe width of $150 \mu\text{m}$. A native oxide was grown outside the

stripe region and covered with 50 nm Ni and 50 nm of Au. The grating etch depth was 100 nm for wafer #734 and 220 nm for wafer #759.

Lasers fabricated from both wafers did not lase. We believe the reason for this lack of successful performance was due to high mode loss inherent in the MCTC structure. Although this structure (wafer #759) was designed to minimize the mode loss, there was still a significant mode loss as evidenced by the lasing "turn-off" behavior. Since the α -DFB laser requires the two lateral modes to be degenerate, this loss could break the degeneracy and cause the laser not to function as desired. The α -DFB laser requires κ values (and effective refractive index differences) significantly larger than standard DFB lasers. In order to achieve these large κ values using the MCTC structure, the design is such that large effective refractive index differences are necessarily accompanied by high mode loss. Ultimately, the high mode loss inherent in the MCTC structure may prove to prohibit the fabrication of MCTC α -DFB lasers.

Conclusions

The main conclusions of this research effort on the use of the modulated cap, thin p-clad (MCTC) design to fabricate semiconductor lasers with improved spatial and spectral beam qualities are as follows:

1. The MCTC design applied to antiguided array lasers has great promise based on the initial device performance obtained in Phase I of the contract and the simplicity of the fabrication scheme. The "process window" concept utilized in Phase II indicates that it should be possible to make MCTC antiguided arrays with high yield provided the epitaxial material utilized is very uniform and the high loss concept proposed can be realized.
2. The pulsed anodization/etching technique utilized in fabricating the MCTC antiguided array lasers can produce the precise etch depths required to achieve the device design requirements. Its simplicity and reproducibility compared to other etching techniques indicates that it could prove to be of great value in the semiconductor processing industry.
3. The failure of the MCTC, α -DFB laser designs utilized in the study and the modeling work done lead us to conclude that the MCTC design concept is not useful for fabricating α -DFB lasers. We do believe however that the MCTC design is potentially very useful in fabricating conventional in-plane DFB lasers and grating surface emitters capable of high power, single-lobe beam operation.

Bibliography

1. "Microsecond-long Lasing Delays in Thin P-clad InGaAs QW Lasers", C.H. Wu, C.F. Miester, and P.S. Zory, IEEE/LEOS '96 Conference Proceedings, Boston, MA (November 1996)
2. "Thermally Induced Delayed Turn-On in Thin P-Clad Lasers", C.F. Miester, C.H. Wu, and P.S. Zory, SPIE Proceedings 3001, pp 177-183 (February 1997)
3. "Anomalous Behavior of Strained InGaAs Quantum Well Lasers", C.F. Miester, C.H. Wu and P.S. Zory, 25th Annual AVS Symposium, Orlando, FL (February, 1997)
4. "Modulated-Cap Thin P-Clad Lasers", P.S. Zory, J.S. O, C.F. Miester, J. Yoon and M.A. Emanuel, DLTR Technical Digest, pp 15-17, Albuquerque, NM (June 1997)
5. "Modulated-Cap Thin P-Clad Antiguided Array Lasers", J.S. O, P.S. Zory, C.F. Miester, J. Yoon, M.A. Emanuel, V.R. Sperry, B.D. Schwartz, and R. Setzko, SPIE Proceedings, 3284 pp 36-40 (January 1998)
6. "Modulated-Cap Thin P-Clad Lasers", P.S. Zory, J.S. O, C.F. Miester, J. H. Han, M. J. Kasraian, B.D. Schwartz and R. Setzko, DLTR Technical Digest, Albuquerque, NM (March 1998)
7. "Fabrication of Antiguide Array Lasers Using a Modulated-Cap Thin P-Clad Structure", J.S. O and P.S. Zory, Proceedings of the Conference on Lasers and Electro-Optics, pp 36-37 (May 1998)

8. "Modulated-Cap Thin p-Clad Antiguided Array Lasers", J.S.O, Ph.D. Dissertation, Electrical & Computer Engineering Dept., University of Florida (December 1998)

9. "Antiguided Array Diode Lasers Fabricated with Modulated Cap Thin P-Clad Structure", J.S.O, P.S. Zory, B.D. Schwartz, R. Setzko, M.A. Emanuel and V.R.Sperry, IEEE Phot. Tech. Lett., 11 (April 1999)

DISTRIBUTION LIST

AUL/LSE

Bldg 1405 - 600 Chennault Circle

Maxwell AFB, AL 36112-6424

1 cy

DTIC/OCP

8725 John J. Kingman Rd, Suite 0944

Ft Belvoir, VA 22060-6218

2 cys

AFSAA/SAI

1580 Air Force Pentagon

Washington, DC 20330-1580

1 cy

AFRL/PSTL

Kirtland AFB, NM 87117-5776

2 cys

AFRL/PSTP

Kirtland AFB, NM 87117-5776

1 cy

Peter S. Zory

University of Florida

Department of Electrical and Computer Engineering

319 Weil Hall

P.O. Box 116500

Gainesville, FL 32611-5500

1 cy

Official Record Copy

AFRL/DELS/David Bossert

3 cys